ACS OMEGA

http://pubs.acs.org/journal/acsodf

Article

A Comparative Study of Mechanism and Performance of Anionic and Cationic Dialdehyde Nanocelluloses for Dye Adsorption and Separation

Xiangyu Huang, Pejman Hadi, Ritika Joshi, Abdulrahman G. Alhamzani, and Benjamin S. Hsiao*

Cite This: *ACS Omega* 2023, 8, 8634−8649

Read Online

ACCESS | Metrics & More | Article Recommendations | Supporting Information

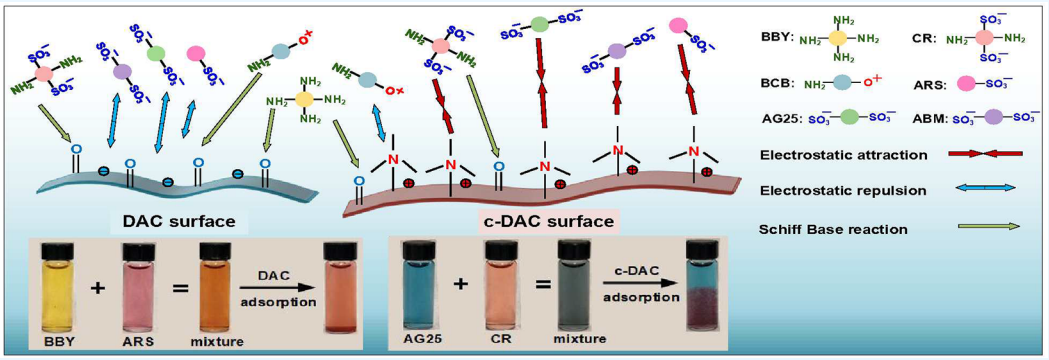

ABSTRACT: In this study, anionic dialdehyde cellulose (DAC) and cationic dialdehyde cellulose (c-DAC) nanofibrous adsorbents were prepared via a two-step reaction from bamboo pulp, using sodium periodate and Girard's reagent T as oxidizing and cationizing agents, respectively. The performance of DAC and c-DAC for selective dye adsorption and separation was evaluated by six different organic dyes (with varying charge properties) and certain binary mixtures. Both adsorbents could remove the dyes but with different capability, where DAC exhibited high adsorption efficiency against cationic dyes (e.g., the maximum adsorption capacity for Bismarck brown Y was 552.1 mg/g) and c-DAC exhibited high adsorption efficiency against anionic dyes (e.g., the maximum adsorption capacity for Congo red was 540.3 mg/g). To investigate the adsorption mechanism for these adsorbents, effects of contact time, initial pH value, initial dye concentration, and ionic strength on the adsorption activity against Congo red were investigated. The adsorption equilibrium data of DAC were found to fit best with the Langmuir isotherm model, whereas that of c-DAC were found to fit best with the Freundlich model. Both DAC and c-DAC adsorption kinetic data could be described by the pseudo-second-order kinetic model, and these adsorbents possessed stable adsorption efficiency in the pH range of 4−10. Furthermore, their dye adsorption capabilities were found to increase with increasing ionic strength (salt concentration). The distinctive complementary features of DAC and c-DAC will allow them to remove a wide range of organic dyes from industrial wastewater.

1. INTRODUCTION

The world is facing pressing water crises because of the rapid decline in available freshwater sources. Dye contamination from manufacturing industries, such as textile, paper, leather, plastic, etc., contributes to this crisis. The effective removal of organic dyes from contaminated industrial wastewater has become an urgent task in addressing this widespread environmental issue. It has been reported that more than 700,000 tons of dyes are produced yearly around the world with over 10,000 tons of dyes consumed in the textile industry, where approximately 10−15% of dyes are leaked into the environment.[1] As most synthetic dyes contain azo linkages and aromatic rings, which make them highly toxic and non-biodegradable, their presence in our hydrosphere can pose a significant threat not only to human health (i.e., carcinogenesis, respiratory toxicity, and teratogenicity) but also to the aquatic ecosystem.[2] To remediate this problem, various biological, chemical, and physical techniques, such as enzyme degradation,[3] photocatalysis,[4] ion exchange,[5] coagulation,[6] membrane filtration,[7] and electrochemical treatment,[8] have been developed to treat dye contamination in wastewater. Among these methods, the adsorption approach is considered

Received: December 8, 2022
Accepted: February 13, 2023
Published: February 23, 2023

https://doi.org/10.1021/acsomega.2c07839
ACS Omega 2023, 8, 8634−8649

a cost-effective approach for dye removal due to the low cost, energy efficiency, and ease of implementation.[9,10]

The most crucial step for the implementation of the adsorption process in wastewater treatment is the development of an efficient, sustainable, and cheap adsorbent. Although numerous low-cost natural adsorbents, such as chitosan,[11] activated carbon,[12] plant gum,[13] graphene,[14] and coffee residue,[15] have been reported in recent years, these materials still have some shortcomings that need improvement. For example, some fabrication processes of these adsorbents require the use of undesirable solvents, toxic monomers, and metal catalysts that can create additional pollution issues, and some reactions are too energy-intensive to be cost-effective.[12,13,16] Additionally, very few studies have been carried out to understand the effectiveness of these adsorbents for selection and separation of different dyes. In the textile industry, the selective removal ability of an adsorbent is highly desirable, as sometimes only certain dyes need to be recycled from the effluent. To date, most reported adsorbents that possess effective selective dye adsorption abilities are usually realized by introducing charges on the surface or within the framework of polymers,[10,17] metal−organic frameworks,[18] and alloy[19] adsorbents. However, the high production cost of these materials due to the need for special reagents or processing techniques (e.g., organic solvents, electrospinning, and freeze-drying) have limited their real-world applications.

Micro- and nanoscale cellulose, extracted from abundant and diverse biomass feedstocks, are widely used as green and sustainable adsorbents for water purification.[20] In recent studies, various functional groups or grafted oligomers/polymers, such as aminosilane,[21] imidazolium ionic liquids,[22] zwitterion moieties,[23] and polyethylenimine,[24] have been attached to the cellulose surface for the effective removal of organic dyes. The adsorption takes place due to the strong electrostatic interaction between the dye molecules and the modified cellulose surface. However, there are few studies regarding the application of nanocellulose-based adsorbents for selective adsorption and separation of cationic and anionic dyes through multiple interaction forces.

In this study, we report a relatively simple and cost-effective approach to prepare two types of nanocellulose-based adsorbents with either a negatively charged or positively charged surface for adsorption and selective separation of organic dyes. Specifically, partially fibrillated nanostructured dialdehyde cellulose (DAC) with an anionic surface was first produced through periodate oxidation. Subsequently, cationic dialdehyde nanocellulose (c-DAC) was prepared by cationizing DAC using (carboxymethyl)trimethylammonium chloride hydrazide (Girard's reagent T), containing both amino and quaternary ammonium groups. Girard's reagent T has a long history in the preparation of cationic dialdehyde starch[25] and has also been used as an effective agent for cellulose cationization.[26,27] To the best of our knowledge, no studies have ever been reported on the investigation of anionic and cationic dialdehyde celluloses for dye separation and selection, nor on the examination of complex multiforce driven adsorption between dialdehyde cellulose adsorbents and dye molecules. Thus, in this study, the adsorption behavior of the resulting DAC and c-DAC adsorbents against different varying cationic and anionic organic dyes and their mixtures was systematically explored. It was found that DAC exhibited high and selective uptake capability toward cationic dyes over anionic dyes, whereas c-DAC showed an opposite trend. In addition, Congo red was chosen as a model dye to further evaluate the effects of experimental factors on the adsorption behavior, possible mechanism, recyclability, and a possible implementation pathway by dynamic column adsorption.

2. EXPERIMENTAL SECTION

2.1. Chemicals and Materials. Bamboo pulp was used as the biomass source in this study. Sodium periodate ($NaIO_4$, 99%), alizarin red S (ARS), and brilliant cresyl blue (BCB) were purchased from Acros Organics. (Carboxymethyl)-trimethylammonium chloride hydrazide (Girard's Reagent T, 99%) and acid green 25 (AG25) were purchased from Sigma-Aldrich. Sodium hydroxide (NaOH, 97%), hydrochloric acid (HCl, 36.5−38%), sodium chloride (NaCl, 99%), sodium sulfate (Na_2SO_4, 99%), sodium phosphate (Na_3PO_4, 96%), hydroxylamine hydrochloride ($NH_2OH{\cdot}HCl$, 96%), and dehydrated alcohol (CH_3CH_2OH, 99.5%) were purchased from Fisher Scientific. Congo red (CR), Bismarck brown Y (BBY), and acid brown M (ABM) were purchased from Alfa Asear. All chemicals were used as received without further purification.

2.2. Preparation of Anionic and Cationic Dialdehyde Cellulose Adsorbents. *2.2.1. Anionic Dialdehyde Cellulose (DAC).* DAC was prepared by adding sodium metaperiodate ($NaIO_4$/dried cellulose ratio was 4 mmol/g) into a 1.25 wt% bamboo pulp (pristine_cellulose) suspension. The reaction was heated at 55 °C for 24 h without any exposure to light. After the reaction finished, the formed iodate was regenerated back to periodate using 1.25 M hypochlorite solution under the alkaline condition, according to a method reported by Liimatainen et al.[28] The resulting partially fibrillated DAC microfibers were subsequently washed with DI water followed by vacuum filtration until the conductivity of the filtrate became lower than 5 μS/cm.

2.2.2. Cationic Dialdehyde Cellulose (c-DAC). The c-DAC adsorbent was prepared by modifying the DAC sample with Girard's reagent T (GT) as described in our previous study.[27] In brief, GT was dissolved into the DAC suspensions with a GT/anhydroglucose mole ratio of 3:1; the pH value of the mixture was then adjusted to 4.5 using 0.1 M HCl solution. The reaction was allowed to proceed for 72 h under continuous stirring at room temperature. The resulting c-DAC suspension was transferred into dialysis tubing (Spectral/Por, 3.5 kDa MWCO) in a deionized water bath until the conductivity of the water bath was below 5 μS/cm. Both DAC and c-DAC samples were stored at 4 °C in suspension form for further study.

2.3. Material Characterization. *2.3.1. Determination of Aldehyde and Nitrogen Content.* The aldehyde content on DAC and c-DAC samples was determined using the hydroxylamine hydrochloride titration method.[29] The nitrogen content of c-DAC was determined using the CNS (carbon, nitrogen, and sulfur) elemental analysis technique (Thermo Scientific, EA1112). Detailed calculation methods of the aldehyde content and GT's degree of substitution are described in the Supporting Information (sections S1 and S2).

2.3.2. Chemical and Crystalline Structure Characterizations. The functional groups of pristine_cellulose, DAC, and c-DAC samples were characterized by Fourier transform infrared (FTIR) spectroscopy (Thermo Scientific, Nicolet iS10), where the spectra were obtained at a resolution of 4 cm^{-1} in the wavenumber range of 700−4000 cm^{-1}. Solid-state ^{13}C cross-polarization/magic angle spinning nuclear magnetic

https://doi.org/10.1021/acsomega.2c07839
ACS Omega 2023, 8, 8634−8649

resonance (CPMAS NMR) spectroscopy was conducted using a Bruker AVANCE III HD 600 MHz NMR spectrometer. All samples were tested at a spinning speed of 11.7 kHz with a minimum of 24,000 scans. The crystalline diffraction profiles were obtained by wide-angle X-ray diffraction (WAXD, Rigaku, Benchtop MiniFlex 600) using a Cu Kα radiation source (λ = 1.5406 Å) operated at 40 kV and 15 mA. The 2θ diffraction diagrams were obtained between 5° and 40° at a scanning rate of 5° min^{-1}. The peak deconvolution analysis was carried out to calculate the crystallinity index (CI) and crystallite dimensions of the sample.[30] In this analysis, the sharp crystal diffraction peaks in the WAXD profile was fitted with the pseudo-Voigt function using MDI Jade 10 software (Materials Data, Inc.), and the broad amorphous background (at around 21.5°) was fitted with the Gaussian function. The CI value was determined by the ratio between the sum of the area under the crystal diffraction peaks over the total area under the WAXD profile. The crystal dimensions of the major lattice planes were also estimated from the WAXD profiles using Scherrer's equation (eq 1):[31]

$$D_{hkl} = \frac{k\lambda}{B_{hkl}\cos\theta} \quad (1)$$

where k is the Scherrer constant (k = 0.9), λ is the X-ray wavelength (λ = 0.154 nm), B_{hkl} is the peak width at half-maximum intensity, and θ is the diffraction angle.

2.3.3. Surface Characterization of DAC and c-DAC in Solid and Suspension. The surface morphology of DAC and c-DAC samples was characterized by a scanning electron microscopy instrument (SEM, Zeiss, LEO 1550 SFEG) equipped with energy-dispersive X-ray analysis (EDX) for elemental mapping (EHT = 2.5 kV). TEM images of these samples were acquired using a transmission electron microscopy instrement (TEM, JEOL, JEM-1400) operated at 80 kV. The sample preparation for TEM measurements was as follows: DAC and c-DAC suspensions were diluted to 0.01 wt % and subsequently sonicated for 1 h. Then, 10 μL of suspension was deposited onto a carbon-coated 300-mesh copper grid (Ted Pella Inc.), followed by staining using a drop of 2.0 wt% uranyl acetate for 10 s. The Brunauer–Emmett–Teller (BET) specific surface areas of DAC and c-DAC were analyzed via the N_2 adsorption–desorption isotherms using a NOVAtouch LX2 (Quantachrome) instrument. The zeta potentials of DAC and c-DAC suspensions (0.1 wt%) were measured via a Zetaprobe analyzer (Colloidal Dynamics) to investigate their surface charge.

2.4. Dye Adsorption Studies. The following adsorption studies were conducted in triplicate at room temperature (25 ± 1 °C) with the samples being shaken at 250 rpm in darkness to complete the adsorption process. Both DAC and c-DAC adsorbents were tested in the suspension form.

2.4.1. Dye Selective Adsorption Study. To evaluate the selective adsorption efficiencies of DAC and c-DAC, batch adsorption tests were carried out using both cationic dyes (BBY and BCB) and anionic dyes (CR, AG25, ABM, and ARS). All the experiments in this section were performed using a single-component dye system. Before the adsorption test, calibration curves of each dye were obtained using UV–vis spectroscopy (Thermo Scientific, Genesys 10S), and the results are shown in Figure S1. The equilibrium adsorption value (q_e) of DAC and c-DAC against each individual dye was obtained by the typical adsorption test as follows: an appropriate amount of DAC or c-DAC suspension (equivalent to 7.5 mg in dry weight) was added to an aqueous dye solution to prepare a 15 mL testing solution (the initial concentration C_0 = 100 mg/L, pH 7). The mixture was oscillated for 24 h to reach equilibrium. After centrifuge separation of the cellulose adsorbent from the dye solution, the final concentration of the dye solution was determined via UV–vis spectroscopy at the maximum adsorbance value of each dye (i.e., $\lambda_{max\text{-}BBY}$ = 463 nm, $\lambda_{max\text{-}BCB}$ = 625 nm, $\lambda_{max\text{-}CR}$ = 497 nm, $\lambda_{max\text{-}AG25}$ = 610 nm, $\lambda_{max\text{-}ABM}$ = 464 nm, and $\lambda_{max\text{-}ARS}$ = 516 nm). The amount of the dye adsorbed by the DAC or c-DAC adsorbent, q_e (mg/g), was determined by eq 2:

$$q_e = \frac{(C_0 - C_e)V}{m} \quad (2)$$

where C_0 and C_e (mg/L) are the initial and final concentrations of the dye in aqueous solution, respectively; V (L) is the solution volume; and m (g) is the mass of the adsorbent used.

2.4.2. Mixed Dye Separation Study. The separation of dye mixtures by DAC and c-DAC was also investigated. All the experiments in this section were performed using a binary-component dye system. Specifically, 7.5 mg of DAC was added into 15 mL of an aqueous mixture of BBY and ARS, whereas 7.5 mg of c-DAC was added into 15 mL of an aqueous mixture of CR and AG25. The initial concentration of all dyes in the mixture was 25 mg/L. After being oscillated for 5 h, the mixtures were centrifuged; the supernatants were then analyzed by UV–vis spectroscopy in the wavelength range of 400–700 nm with medium rate scanning.

2.4.3. Effects of Experimental Factors on the Adsorption Performance. As the typical dye molecule often contains both amino groups and sulfonate groups, CR was chosen as a model dye in this study to investigate the adsorption mechanism, kinetics, isotherms, and optimum adsorption conditions for the DAC and c-DAC adsorbents. The following factors were carefully evaluated. All the experiments in this section were performed using a single-component dye system.

Adsorption Kinetic Study. In this study, 2.5 mg of DAC or c-DAC adsorbent was used to treat the CR aqueous solution (5 mL, C_0 = 100 mg/L, pH 7). The CR concentrations were determined at different time intervals (10–480 min). The dye uptake (q_t) was then plotted against the contact time (t) and analyzed using the pseudo-first-order, pseudo-second-order, and intraparticle diffusion models to obtain the kinetic adsorption parameters.

Effect of pH. The effect of the initial pH value on the equilibrium CR adsorption value was investigated by adding 2.5 mg DAC or c-DAC into 5 mL of CR solution (C_0 = 100 mg/L) at different pH values (4–12). In this experiment, the mixture was equilibrated for 24 h before testing.

Effect of Initial Dye Concentration on Adsorption Isotherm. The adsorption isotherm of DAC and c-DAC adsorbent was studied by adding 2.5 mg of adsorbent into a 5 mL of CR aqueous solution (C_0: 50–2000 mg/L, pH 7) or BBY aqueous solution (C_0: 10–300 mg/L, pH 7), whereby the mixture was centrifuged and analyzed after 24 h. The equilibrium dye uptake (q_e) was plotted against the equilibrium concentration (C_e) and fitted by three different isotherm models (i.e., Langmuir, Freundlich, and Temkin models) for analysis.

Effect of Ionic Strength. The effect of different coexisting anions (NO_3^-, SO_4^{2-}, and PO_4^{3-}) was investigated at a series

https://doi.org/10.1021/acsomega.2c07839
ACS Omega 2023, 8, 8634–8649

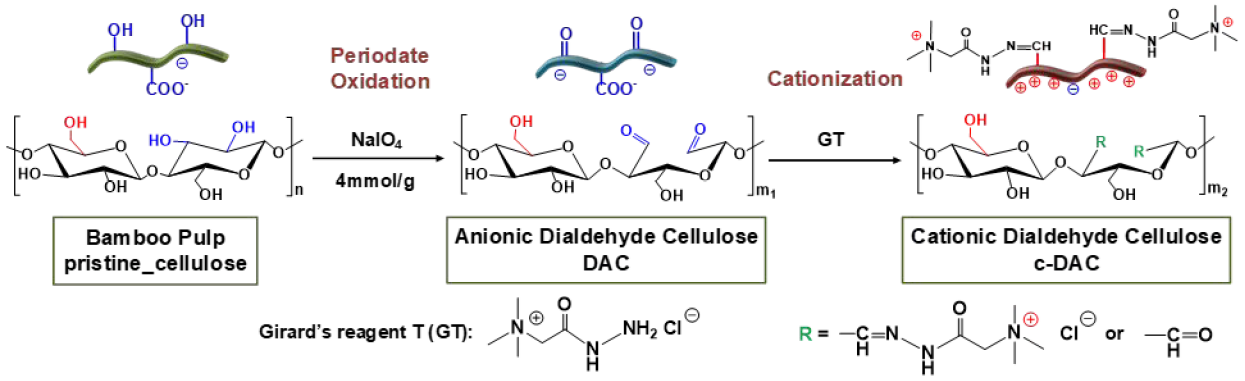

Figure 1. Preparation of DAC by periodate oxidation of bleached pulp and subsequent cationization using Girard's reagent T to create c-DAC.

Table 1. Surface Characteristics of Pristine_Cellulose, DAC, and c-DAC Samples

		average % (w/w)					
sample	aldehyde content(mmol/g)	N	C	S	GT content(mmol/g)	DS %	zeta potential (mV)
pristine_cellulose		0.00	40.45	0.07	0.00	0	
DAC	5.27	0.00	38.34	0.10	0.00	0	−24.2 ± 3.0
c-DAC	1.35	0.63	40.10	0.10	0.14	2.73	+40.8 ± 3.5

of concentrations (i.e., 0.01, 0.05, 0.1, 0.2, and 0.3 M) using 2.5 mg of adsorbent and 5 mL of CR solution (C_0 = 100 mg/L, pH 7, 24 h).

2.4.4. Recyclability Test. The recyclability of c-DAC toward cationic dye adsorption was evaluated via five consecutive adsorption−desorption cycles. In this experiment, a mixture of 99.5% ethanol and 0.1 M NaOH (1,1 volume ratio) was prepared as the eluent to recover the adsorption sites on c-DAC. Specifically, the desorption process was performed by separating 15 mg of CR-loaded c-DAC from the batch adsorption via vacuum filtration of the mixture prepared under vigorous stirring for 30 min. Then the eluent with desorbed CR was analyzed via UV−vis to estimate the desorption efficiency. In each cycle, 30 mL of CR solution (C_0 = 100 mg/L, pH 7) was used in the adsorption test, while 30 mL of the eluent was used for the desorption test. Each adsorption or desorption run lasted for 30 min.

2.4.5. Column Adsorption Test. Column adsorption experiments were carried out at room temperature (25 ± 1 °C) in a glass column having an inner diameter of 3.2 cm. In this experiment, 0.5 g of freeze-dried DAC or c-DAC sample was loaded into the column, forming a fixed bed with a 3 cm bed height. The dynamic adsorption experiment was conducted by pumping a CR solution (C_0 = 100 mg/L, pH 7) upward through the column bed at a flow rate (Q) of 2 mL/min. The effluent sample was collected at a fixed time interval. The CR concentration in the effluent was analyzed by UV−vis. The breakthrough curve was obtained by plotting the ratio of C_t/C_0 against time (t), where C_t and C_0 (mg/L) are the dye concentrations in the effluent and influent, respectively. The experiment was stopped when the column reached the saturation point.

According to the experimental data, the column maximum adsorption capacity and other relevant parameters in the column adsorption process could be analyzed as follows.[32,33] For a given influent concentration and flow rate, the column maximum adsorption capacity q_{tot} (mg) can be obtained using eq 3:

$$q_{tot} = \frac{QA}{1000} = \frac{Q}{1000}\int_{t=0}^{t=t_{tot}} C_{ads}\,dt \quad (3)$$

where A is the area under the breakthrough curve, Q (mL/min) is the flow rate, t_{tot} (min) is the total flow time, and C_{ads} = $C_0 - C_t$ (mg/L) is the concentration of the adsorbed CR. The amount of the dye adsorbed per unit weight of the adsorbents in column adsorption, column equilibrium capacity q_{eq} (mg/g), can be calculated by eq 4.

$$q_{eq} = \frac{q_{tot}}{m} \quad (4)$$

where m (g) is the amount of the adsorbent loaded in the column bed. The total amount of the dye infused in the column M_{tot} (mg) can be calculated by eq 5.

$$M_{tot} = \frac{C_0 Q t}{1000} \quad (5)$$

Finally, the removal rate of dye, R (%) can be calculated by eq 6.

$$R = \frac{q_{tot}}{M_{tot}} \quad (6)$$

3. RESULTS AND DISCUSSION

3.1. Preparation and Characterization of DAC and c-DAC Adsorbents. The anionic and cationic dialdehyde cellulose adsorbents were achieved through two consecutive reactions: (1) the oxidation of the hydroxyl groups at C_2 and C_3 positions of the glucose unit on the cellulose surface to obtain DAC and (2) the subsequent Schiff's base reaction between the aldehyde groups on DAC and the amino groups on GT, therefore "chemically grafting" the cationic quaternary ammonium groups onto the cellulose surface and forming c-DAC. We note that the presence of surface charge on cellulose would result in partial fibrillation (or electrostatic swelling) of the pulp. The application of low mechanical energy (e.g., by homogenization) can easily fully fibrillate the pulp and result in a nanofiber dispersion. However, we did not carry out the

https://doi.org/10.1021/acsomega.2c07839
ACS Omega 2023, 8, 8634−8649

mechanical fibrillation step because the partially fibrillated sample in the form of a microfiber greatly facilitates its ability to be handled. The anionic surface charge of DAC can be attributed to the hypochlorite bleaching process of bamboo pulp, converting some hydroxyl groups into carbonyl groups, and subsequently carboxyl groups.[44] Furthermore, in the periodate oxidation step, some dialdehyde groups may be further oxidized and generate dicarboxylic cellulose as the byproduct. The two-step preparation route for creation of DAC and c-DAC and their corresponding structures are shown in Figure 1.

Table 1 summarizes the surface characteristics of pristine_cellulose (bamboo pulp), DAC, and c-DAC samples. Based on the titration study, the values of the aldehyde content in DAC and c-DAC were found to be 5.27 and 1.35 mmol/g, respectively. The smaller aldehyde content in c-DAC could be attributed to the Schiff's base reaction between DAC and GT, where imine bonds were formed between aldehyde and amino groups and some unreacted aldehyde groups could remain in c-DAC. Interestingly, no nitrogen content was detected in pristine_cellulose and DAC samples. However, after treatment with GT, the value of 0.63% nitrogen content in c-DAC corresponds to a 2.73% GT's degree of substitution (DS) per bulk anhydroglucose unit. Furthermore, the zeta potential values of cellulose suspensions also showed a reversed-charge change: −24.2 mV for DAC and +40.8 mV for c-DAC. Both elemental analysis and zeta potential measurement results indicated the successful GT modification on the cellulose surface.

The morphologies of DAC and c-DAC samples were investigated by SEM and TEM techniques, where the results are shown in Figure 2. In the SEM image of DAC (Figure 2a), large fiber bundles were seen, indicating the degree of fibrillation in DAC was low due to the weak electrostatic repulsive interaction on the surface of DAC. The partially fibrillated morphology in DAC could be identified in the TEM image (Figure 2c), exhibiting the dimensions of fibrillated nanofibers (the fiber length in the range of 50−150 nm and the mean fiber width of 4.49 ± 1.14 nm). In contrast, the SEM image of c-DAC (Figure 2b) showed a larger degree of fibrillation, where the corresponding TEM image (Figure 2d) displayed a relatively homogeneous small aggregation of nanofibrils having the fiber length in the range of 150−550 nm and the mean fiber width of 10.41 ± 2.79 nm.

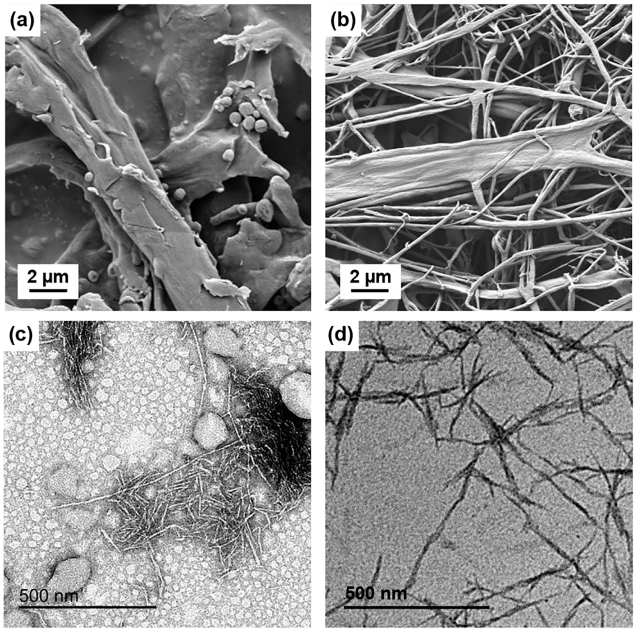

Figure 2. SEM images of (a) DAC and (b) c-DAC and TEM images of (c) DAC and (d) c-DAC.

These results can be explained by the following reasons. The electrostatic repulsion forces between c-DAC fibers can increase significantly by introducing the positively charged quaternary trimethylammonium ($-N^+(CH_3)_3$) groups onto the cellulose surface, facilitating the fibrillation process.[27] This hypothesis was supported by the BET measurement, where the BET specific surface area of DAC was 8.10 m^2/g, but that of c-DAC was 11.93 m^2/g for c-DAC (the curves of nitrogen adsorption−desorption isotherm are shown in Figure S2).

The FT-IR spectra of pristine_cellulose, DAC, and c-DAC samples are shown in Figure 3a. All the spectra exhibited typical characteristic peaks of cellulose at 3332, 2897, 1429, 1367, 1316, 1261, 1161, 1030, and 897 cm^{-1}.[34] The new peaks observed at 1727 and 887 cm^{-1} in the DAC spectrum were assigned to the carbonyl group stretching and the hydrated form of dialdehyde cellulose, respectively, which confirmed the success of periodate oxidation.[35] In the c-DAC spectrum, two new peaks observed at 1686 and 926 cm^{-1} were assigned to the carbonyl group and the N−N bond in the attached GT reagent.[36] Furthermore, the peak at 1595 cm^{-1} could be assigned to the imine bond formed between the aldehyde group on DAC and the GT reagent, further confirming the successful grafting of GT onto the DAC surface.[26,37]

The solid-state ^{13}C NMR spectra were acquired to further investigate the cellulose structural changes by the cationization process (Figure 3b). The characteristic peaks in the pristine_cellulose spectrum were assigned to C_1 (105 ppm), C_4 (89 ppm), C_4' (84 ppm), $C_{2,3,5}$ (70−80 ppm), and C_6 (65 ppm) atoms in the repeating anhydroglucose unit (AGU).[38] In contrast, the DAC spectrum in the range of 100−80 ppm showed a great deal of deterioration, implying a decrease in the ordering of cellulose crystalline structure due to oxidation.[38] Contrary to DAC, the c-DAC spectrum was very similar to the pristine_cellulose spectrum, due to the removal or dissolution of the amorphous region on the DAC surface. A distinctive peak at 56 ppm was observed in the c-DAC spectrum, which could be assigned to the carbon signal in the cationic trimethylammonium group.[39] Furthermore, the absence of an expected carbonyl signal at around 175−180 ppm implies that the aldehyde groups on the cellulose surface were hydrated or existed in the hemiacetal form. Similar observations have been reported previously.[37,40]

The crystalline structure of pristine_cellulose, DAC, and c-DAC were further investigated by the WAXD technique (Figure 3c). All three samples displayed similar diffraction peaks from the cellulose I_β pattern. These peaks appeared at around 14.6°, 16.2°, 22.9°, and 34.5°, which could be attributed to the $(1\bar{1}0)$, (110), (200), and (004) lattice planes, respectively.[41] Based on the deconvolution of the diffractograms (shown in Figure S3), the calculated CI values and the crystal sizes (normal to the three lattice planes of cellulose $(1\bar{1}0)$, (110), and (200)) from the pristine_cellulose, DAC, and c-DAC samples are listed in Table 2.

In Table 2, substantial decreases in the CI value and corresponding crystal size in DAC are observed when compared to those in pristine_cellulose. This could be

https://doi.org/10.1021/acsomega.2c07839
ACS Omega 2023, 8, 8634−8649

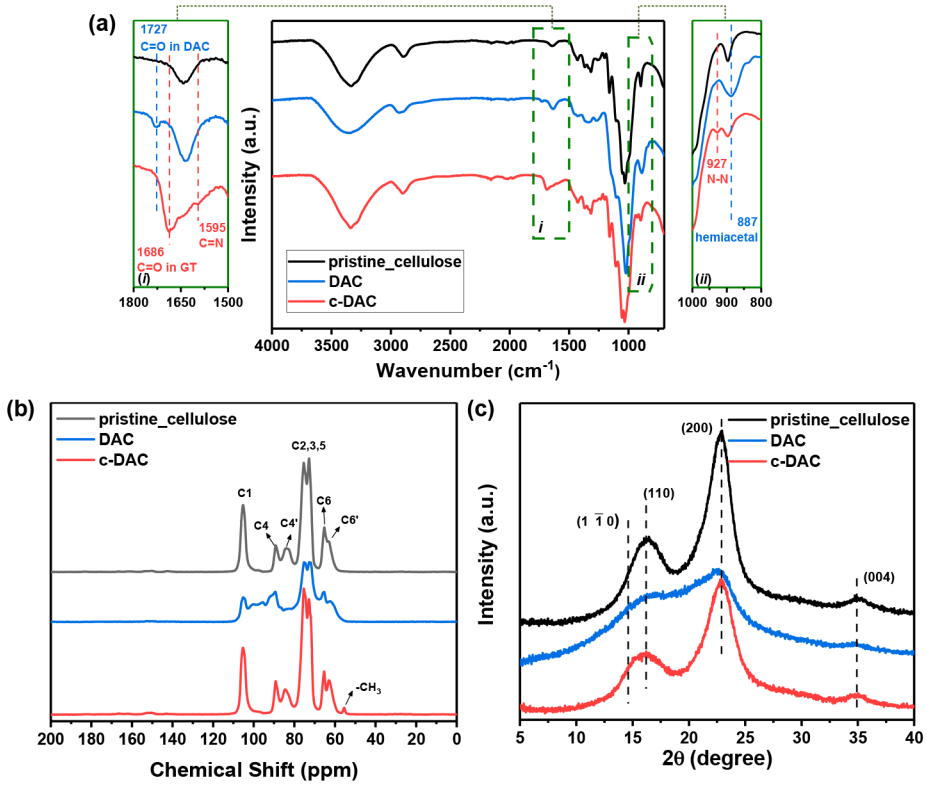

Figure 3. (a) FT-IR spectra and the enlarged regions of interest: (i) 1800−1500 cm^{-1} and (ii) 1000−800 cm^{-1}; (b) the solid-state ^{13}C NMR spectra and (c) WAXD patterns of pristine_cellulose, DAC, and c-DAC samples.

Table 2. Crystalline Index and Crystal Size Normal to the Three Lattice Planes of the Cellulose Crystal Structure from Pristine_Cellulose, DAC, and c-DAC Samples

		crystal size (nm)		
sample	CI (%)	$(1\bar{1}0)$	(110)	(200)
pristine_cellulose	49.6 ± 0.1	2.7 ± 0.1	3.2 ± 0.1	4.1 ± 0.0
DAC	20.7 ± 0.5	1.9 ± 0.1	1.9 ± 0.1	3.6 ± 0.1
c-DAC	47.2 ± 0.3	2.7 ± 0.0	2.8 ± 0.1	3.6 ± 0.1

explained by the opening of the glucose ring, leading to the partial destruction of the ordering in the cellulose crystal structure due to periodate oxidation,[42] which is consistent with the ^{13}C NMR observation. After the cationization process, the WAXD profile of c-DAC became similar to that of pristine_cellulose, where the corresponding CI value increased back to 47.2%. This can be explained by the notion that the cationization process can lead to the breakdown of cellulose chains on the cellulose surface, where some cationic cellulosic derivatives become soluble in water. As a result, some amorphous region was removed and the overall crystallinity of the c-DAC was slightly increased.[27,37] It was interesting to find that the crystal size of the hydrophilic planes $(1\bar{1}0)$ and (110) in c-DAC also showed an apparent increase after cationization. This observation indicated some recrystallization might have occurred on the $(1\bar{1}0)$ and (110) surfaces of the adjacent cellulose microfibrils, similar to the process observed from the drying process.[43]

3.2. Dye Adsorption Studies. *3.2.1. Adsorption of Cationic and Anionic Dyes and Corresponding Adsorption Mechanism.* Two cationic and four anionic dyes were chosen to evaluate DAC and c-DAC's adsorption performance and the corresponding adsorption mechanism. The chemical structures of these six dyes (CR, BBY, AG25, ABM, ARS, and BCB), containing different compositions of positively charged amino or negatively charged sulfonate groups, are illustrated in Figure 4a. The adsorption performance of DAC and c-DAC against these dyes is shown in Figure 5. It was found that DAC showed high q_e value toward cationic dyes (e.g., q_e = 187.6 for BBY and q_e = 13.3 mg/g for BCB). Although DAC also showed appreciable q_e for CR of 30.1 mg/g, its equilibrium adsorption values against other anionic dyes (AG25, ABM, and ARS) were negligible (q_e < 1.6 mg/g). In contrast, c-DAC exhibited high q_e values toward anionic dyes, especially for CR (q_e = 183.6 mg/g). As for cationic dyes, c-DAC adsorbed BBY well (q_e= 66.2 mg/g) but showed no adsorption for BCB. The most significant uptake difference of CR and BBY via c-DAC and DAC could be visually observed (Figure 5b), where the CR and BBY aqueous solutions were almost clear after being adsorbed by c-DAC and DAC, respectively.

Considering the structural differences between DAC and c-DAC on the cellulose surface and the chosen dyes, two possible adsorption mechanisms can be proposed (Figure 4b). In the first mechanism, the dominant adsorption driving forces can be attributed to the formation of covalent bonding between the aldehyde groups on the cellulose surface and the amino groups on the dye by Schiff's base reaction.[44] Thus, it can be rationalized that the adsorption capacity by DAC should decrease in the order BBY > CR > BCB due to the decreasing amino content in these dyes. Moreover, DAC exhibited a higher BBY q_e value than c-DAC because DAC possesses more aldehyde groups on its surface. In the second mechanism, the dominant adsorption driving force can be attributed to the strong electrostatic interaction between the

https://doi.org/10.1021/acsomega.2c07839
ACS Omega 2023, 8, 8634−8649

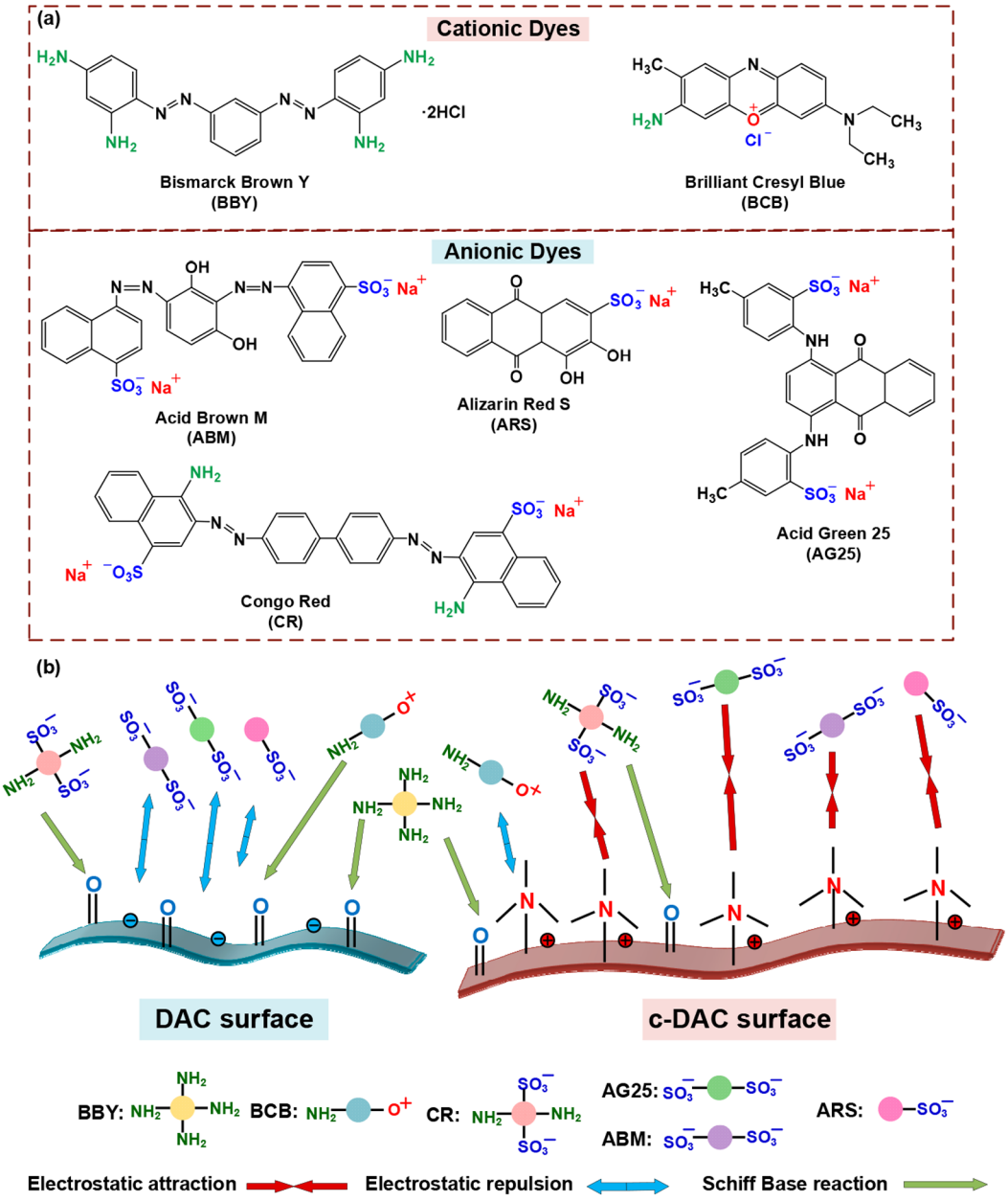

Figure 4. (a) Chemical structures of six tested dyes. (b) Schematics of different dye adsorption mechanisms by DAC and c-DAC adsorbents.

charged cellulose surface and the dye molecules.[45] As DAC's surface is slightly negatively charged, DAC should possess electrostatic attraction to cationic dyes and electrostatic repulsion to anionic dyes.[46] This was observed in this study, which showed that DAC exhibited a higher affinity to cationic dyes over anionic dyes. However, although CR is negatively charged, DAC still displayed adequate adsorption capacity toward it. This can be attributed to the interplay of Schiff's base reaction and electrostatic repulsive force between DAC and CR, in which Schiff's base reaction has played a dominant role. On the other hand, the positively charged surface of c-DAC exhibited higher q_e values for anionic dyes. Due to the dominant attraction forces between the cationic quaternary ammonium groups on c-DAC and the anionic sulfonate groups in dye molecules, the c-DAC's affinity toward anionic dyes was found to increase with the increase of sulfonate contents in dyes, i.e., CR > AG25 ≈ ABM > ARS. However, due to the strong repulsive electrostatic force between c-DAC and cationic dyes, the interaction between c-DAC and some cationic dyes with low amino content (such as BCB) might be low, resulting in little to no adsorption. Meanwhile, c-DAC exhibited some adsorption toward cationic dyes with high amino content (such as BBY). Overall, under the interplay of the above two adsorption mechanisms, DAC is effective for removing cationic dyes having amino groups, while c-DAC is effective for removing anionic dyes.

3.2.2. Selective Separation of Dye Mixture. Based on the different adsorption behaviors toward varying dyes, DAC and c-DAC can be applied in selectively separating different dyes from their mixtures. The expectation is that the dye with a high affinity to the adsorbent (high q_e value) would be adsorbed effectively, while the dye with a low affinity to the adsorbent (low q_e value) would be left in the solution. In order to validate this hypothesis, two binary dye mixtures, BBY−ARS and CR−

https://doi.org/10.1021/acsomega.2c07839
ACS Omega 2023, 8, 8634−8649

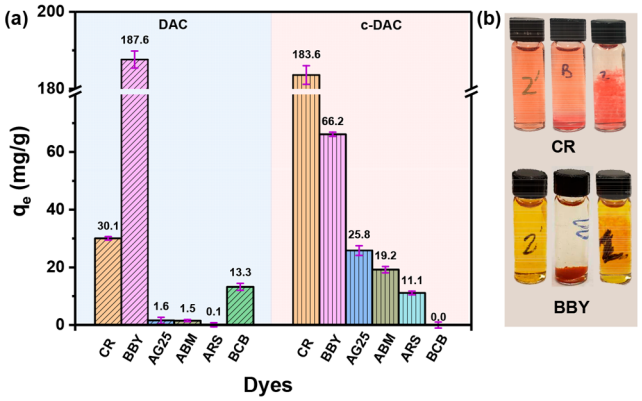

Figure 5. (a) Comparison of DAC and c-DAC's adsorption capabilities toward six different dyes (CR, BBY, AG25, ABM, ARS, and BCB). (b) Photographs of CR and BBY uptake phenomenon, from left to right: the initial dye solution and dye solutions after adsorption via DAC and c-DAC, respectively.

AG25, were chosen as the test models for dye separation tests by using DAC and c-DAC, respectively. The individual dyes and the mixture of dyes before and after adsorption were monitored by both UV−vis spectroscopy and digital images, and the results are shown in Figure 6. In the BBY-ARS mixture, after the adsorption by DAC, the BBY band (λ_{max} = 451 nm) almost disappeared, whereas the intensity of the ARS band (λ_{max} = 516 nm) remained about the same. Moreover, the mixture color faded from orange to pink, which was similar to the color of the pure ARS solution. Similarly, in the AG25-CR mixture, the band of CR (λ_{max} = 497 nm) completely disappeared, and the color of the mixture faded to the same as pure AG25 solution after adsorption by c-DAC. These observations suggest that both DAC and c-DAC adsorb only their high-affinity dyes from the dye mixture and achieve the selective separation of certain dyes.

3.2.3. Effects of Experimental Factors on the Adsorption Performance. Due to the unique structure of CR, which contains both amino and sulfonate groups, CR adsorption can be dominated either by Schiff's base reaction or by electrostatic attraction. For this reason, CR was chosen as a model dye in this study to understand the effects of various experimental factors on the adsorption performance.

The Adsorption Kinetic Study. The CR adsorption kinetics results by DAC and c-DAC were measured at various time intervals from 10 to 480 min (Figure 7a). It was found that the CR adsorption process by c-DAC was rapid in the first 10 min, rapidly approaching the final q_e value of 172 mg/g (i.e., 97% of CR removal). Meanwhile, the CR adsorption by DAC was found to increase relatively slower, with q_e reaching a plateau value of 37 mg/g over about 5 h. These CR adsorption kinetics data were fitted by three kinetic models: (i) pseudo-first-order, (ii) pseudo-second-order, and (iii) intraparticle diffusion, which are expressed in eqs 7, 8, and 9, respectively:[47]

pseudo-first-order:

$$\ln(q_e - q_t) = \ln q_e - K_1 t \tag{7}$$

pseudo-second-order:

$$\frac{t}{q_t} = \frac{1}{q_e} t + \frac{1}{K_2 q_e^2} \tag{8}$$

intraparticle diffusion:

$$q_t = K_{id}(t)^{0.5} + C_i \tag{9}$$

where q_e (mg/g) and q_t (mg/g) are the amounts of adsorbed CR per unit weight of adsorbent at equilibrium and at time t, respectively; K_1 (min^{-1}), K_2 (g mg^{-1} min^{-1}), and K_{id} (mg g^{-1} min$^{-0.5}$) are the rate constants of the pseudo-first-order, the pseudo-second-order, and the intraparticle diffusion models, respectively; and C_i (mg/g) is the intercept constant that relates to the thickness of the boundary layer. The linear fitting results by using these models are shown in Figure 7, and the corresponding kinetic parameters are summarized in Table 3.

From the fitting analysis in Figure 7, it was found that both CR adsorption results using DAC and c-DAC correlated best with the pseudo-second-order model (the correlation coefficient $R^2 \geq 0.999$), considering the results from the other two models. Furthermore, the calculated theoretical equilibrium adsorption values from the pseudo-second-order model ($q_{e,2}$) for DAC and c-DAC agreed very well with the experimental values ($q_{e,exp}$). These results suggest that the

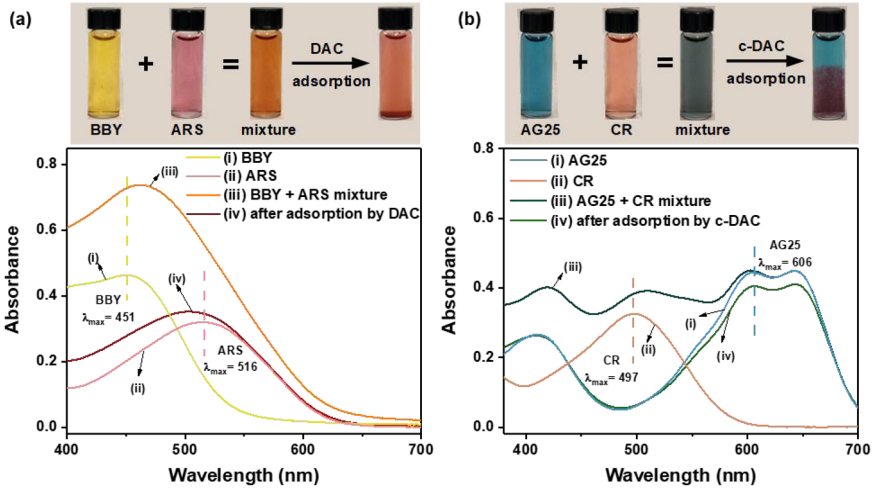

Figure 6. Photographs and UV−vis spectra of (a) BBY-ARS and (b) AG25-CR dyes and their binary mixtures before and after the adsorption by DAC and c-DAC, respectively.

https://doi.org/10.1021/acsomega.2c07839
ACS Omega 2023, 8, 8634−8649

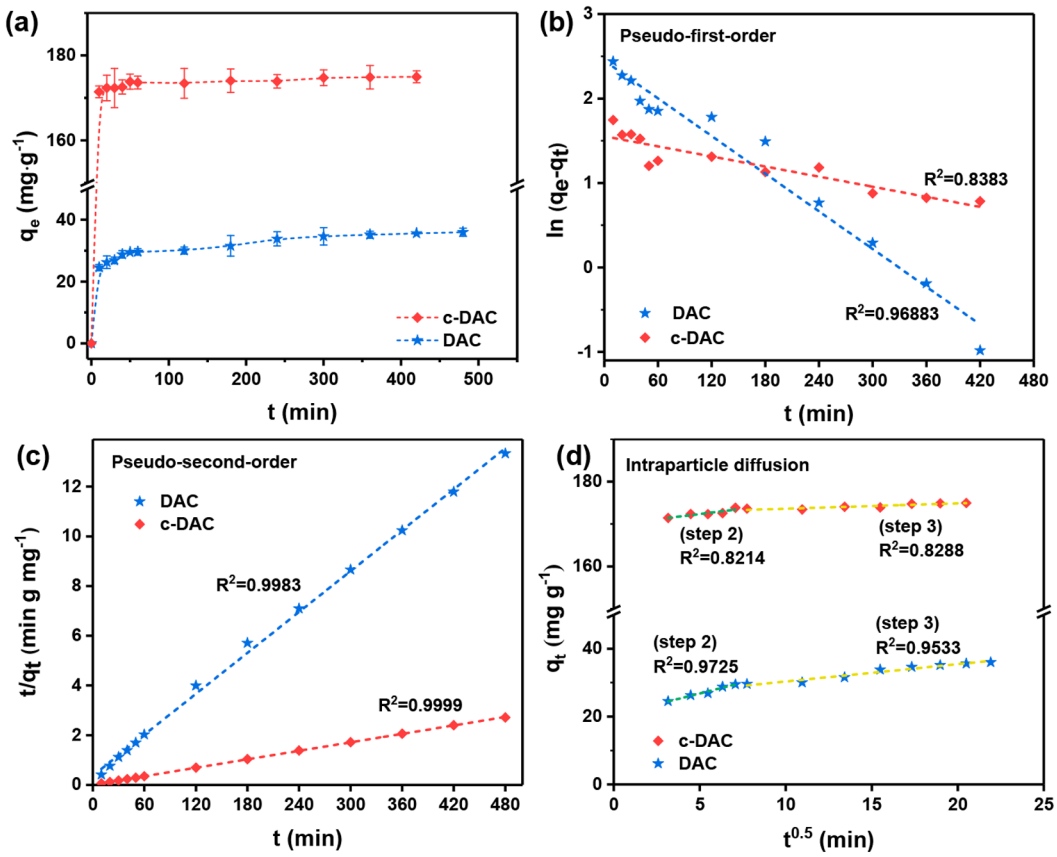

Figure 7. (a) Time evolution of CR adsorption by DAC and c-DAC and the kinetic model fittings using (b) pseudo-first-order, (c) pseudo-second-order, and (d) intraparticle diffusion models.

Table 3. Parameters of Different Kinetic Model Fittings for CR Adsorption onto DAC and c-DAC

kinetic model	equation		parameters	DAC	c-DAC
–	–		$q_{e,exp}$ (mg/g)	36.00	177.16
pseudo-first-order	$\ln(q_e - q_t) = \ln q_e - K_1 t$		$q_{e,1}$ (mg/g)	11.25	2.91
			K_1	7.44×10^{-3}	1.99×10^{-3}
			R^2	0.97	0.84
pseudo-second-order	$\frac{t}{q_t} = \frac{1}{q_e}t + \frac{1}{K_2 q_e^2}$		$q_{e,2}$ (mg/g)	35.44	175.65
			K_2	2.03×10^{-3}	5.07×10^{-3}
			R^2	0.999	1.000
intraparticle diffusion	$q_t = K_{id}(t)^{0.5} + C_i$	step 2	K_{id}	1.28	0.51
			C_i	20.43	169.80
			R^2	0.97	0.82
		step 3	K_{id}	0.51	0.13
			C_i	25.25	172.35
			R^2	0.95	0.83

overall adsorption kinetics of CR onto cellulose adsorbents is dominated by chemisorption, depending on adsorbent and adsorbate.[10,48] This also agrees with our hypothesis that both Schiff's base reaction and electrostatic interaction can happen, where the dominant force can alternate between the electron exchange or electron sharing between CR and cellulose.[49]

We note that the intraparticle diffusion model was also applied to explore the dye diffusion process in the adsorption study, with the results warranting some discussion. The intraparticle diffusion process involves three consecutive steps. Step 1 is relatively sharper, representing the rapid external diffusion of the dye molecules from the bulk solution onto the exterior surface of the adsorbent. Step 2 is an intraparticle diffusion of the dye molecules into the pores of the adsorbent. Step 3 indicates the sorption of the adsorbate onto the active sites on the interior surface of the adsorbent.[49] In Figure 7d, two linear segments with different slopes are shown for both DAC and c-DAC, corresponding to step 2 (CR molecules transport into the macropores of cellulose fibers) and step 3 (dynamic adsorption−desorption equilibrium was achieved), respectively.[50] However, the expected steep step 1 was not observed in this plot (Figure 7d). This might be

https://doi.org/10.1021/acsomega.2c07839
ACS Omega 2023, 8, 8634−8649

because the exterior diffusion of CR molecules occurred too rapidly (less than 10 min), whereas the adsorption study did not capture the initial step 1 stage. It was interesting to find that all fitted lines' intercepts were nonzero ($C_i \neq 0$), indicating that the intraparticle diffusion was not the rate-controlling step, and the CR adsorption process on the cellulose surface could be affected by multiple adsorption mechanisms.[27]

Effect of pH. The pH value of the solution is an important variable affecting the charge of both cellulose adsorbent surface and CR molecules. For this reason, the zeta potential values of the adsorbents under different pH values were measured to determine the optimum pH level for adsorption (the results are shown in Figure 8). Generally, the surface charge of the

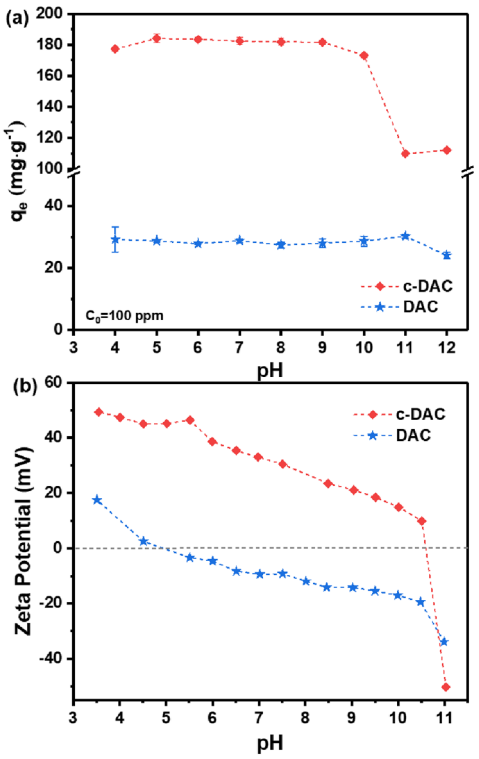

Figure 8. (a) Effect of pH on the adsorption of CR onto DAC and c-DAC adsorbents and (b) zeta potential of DAC and c-DAC suspensions.

adsorbent and adsorbate depends on the protonation or deprotonation of the functional groups.[24] It has been reported previously that the CR molecule typically has a pK_a value of 4.5−5.5, indicating that CR is negatively charged when the pH value is above 5.5 due to deprotonation.[51] Figure 8b is the zeta potential results for both DAC and c-DAC. In c-DAC, the surface charge gradually decreased with the pH value but remained positively charged until the pH value reached 10.5. At pH 11, the zeta potential of c-DAC quickly dropped to a negative value (−50.3 mV). The pH-resistant characteristics of c-DAC can be attributed to the quaternary ammonium groups ($-N^+(CH_3)_3$) on its surface, which is positively charged and relatively pH-independent. Consequently, the strong electrostatic attraction between CR and c-DAC dominated the adsorption process at pH between 4−10, exhibiting the q_e value of 184.1 mg/g at pH 5.0. With the pH value increased to 11, c-DAC exhibited a charge reversal, resulting in a sharp decrease of the CR adsorption value (Figure 8a). In contrast, DAC's adsorption behavior was less pH-dependent, exhibiting only a slight fluctuation between 27.4 and 30.2 mg/g when the pH value increased from 4 to 11. This is because the adsorption mechanism of CR onto DAC is dominated by Schiff's base reaction, which is efficient at low pH (<4) and exceptionally efficient at high pH conditions (>10) but not so much in the tested pH range.[52] It was noted that both DAC and c-DAC still possessed appreciable CR adsorption values under extreme alkalinity (i.e., pH 11−12). This indicates that the electrostatic interaction and Schiff's base reaction mechanism are not the only adsorption mechanisms; the potential adsorption processes through hydrogen bonding and van der Waals force are also present.[53]

Effect of Initial Dye Concentration on Isotherm Study. The effects of the initial CR concentration on the adsorption performance by cellulose adsorbents are shown in Figure 9a. It was observed that with the initial CR concentration being increased from 50 to 2000 mg/L, the q_e value of DAC increased from 18.4 to 129.6 mg/g, while that of c-DAC increased from 98.2 to 540.3 mg/g. This is expected since the large concentration gradient of the adsorbate can increase the mass transfer driving force in the system and result in a higher q_e value.[54]

To further analyze the adsorption of CR molecules on the adsorbent (DAC or c-DAC) surface, three isotherm models (Langmuir, Freundlich, and Temkin) were applied to fit the equilibrium adsorption data. These models can be expressed by eqs 10−12, respectively:[55]

Langmuir:

$$\frac{C_e}{q_e} = \frac{C_e}{q_{max}} + \frac{1}{K_L q_{max}} \quad (10)$$

Freundlich:

$$\log q_e = \log K_F + \frac{1}{n}\log C_e \quad (11)$$

Temkin:

$$q_e = \beta_1 \ln K_T + \beta_1 \ln C_e \quad (12)$$

where C_e (mg/L) is the equilibrium CR concentration, q_e (mg/g) is the amount of the CR adsorbed at the equilibrium concentration, q_{max} (mg/g) is the theoretical maximum adsorption capacity of CR, K_L (L mg^{-1}) is the Langmuir constant, K_F (mg^{1-n} L^n g^{-1}) is the Freundlich constant, and $1/n$ is the adsorption intensity; β_1 (J/mol) is the Temkin constant related to the heat of adsorption, and K_T (L mg^{-1}) is the Temkin equilibrium binding constant. The plots of three isotherm models' linear fitting results are shown in Figure 9, and the relevant parameters from these fits are also listed in Table 4 (the isotherm data presented in this table were calculated by the linear fitting).

According to the correlation coefficient values in Table 4, it could be concluded that the DAC equilibrium adsorption data was best fitted by the Langmuir model (R^2 = 0.99), whereas the c-DAC equilibrium data was best fitted by the Freundlich model (R^2 = 0.99). This was also seen in Figure 9, where the experimental adsorption data of DAC and c-DAC could be well described by the Langmuir model and Freundlich model, respectively. Based on the assumptions for the Langmuir and Freundlich isotherm models, it could be proposed that a homogeneous distribution of CR onto the DAC surface was formed by monolayer adsorption, whereas the adsorption of

https://doi.org/10.1021/acsomega.2c07839
ACS Omega 2023, 8, 8634−8649

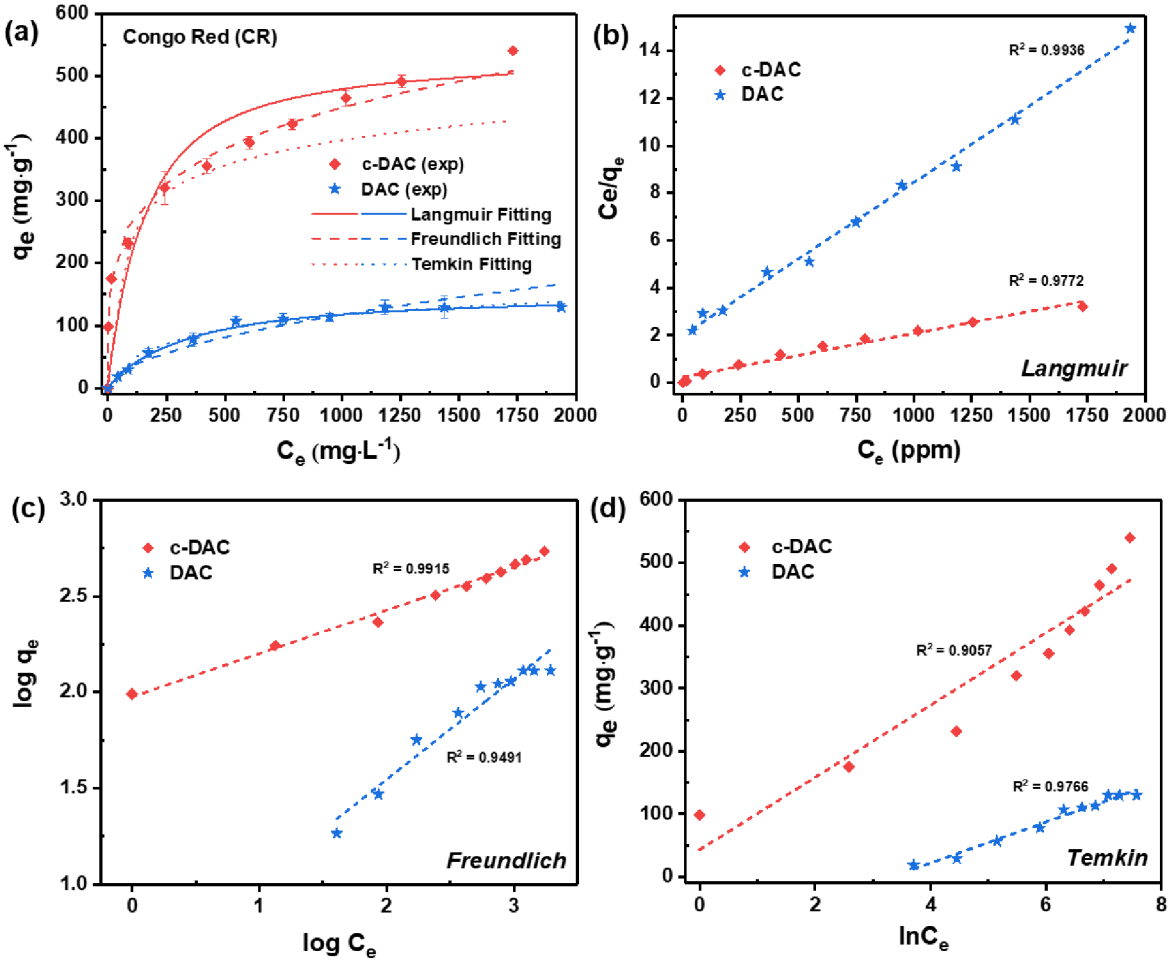

Figure 9. (a) Isotherm adsorption results of Congo red (CR) by DAC and c-DAC adsorbents and their correlations with three different isotherm models (Langmuir, Freundlich, and Temkin). The Langmuir (b), Freundlich (c), and Temkin (d) isotherm models fittings of the isotherm adsorption data.

Table 4. Parameters of Different Isotherm Model Fittings for Adsorption of CR on DAC and c-DAC

model	equation	parameters	DAC	c-DAC
–	–	$q_{max,exp}$ (mg/g)	129.6	540.3
Langmuir	$\frac{C_e}{q_e} = \frac{1}{q_{max}}C_e + \frac{1}{K_L\, q_{max}}$	q_{max} (mg/g)	154.8	540.5
		K_L (L mg^{-1})	3.23×10^{-3}	7.87×10^{-3}
		$R_L = \frac{1}{1 + K_L C_0}$	0.13–0.86	0.06–0.72
		R^2	0.99	0.98
Freundlich	$\log q_e = \log K_F + \frac{1}{n}\log C_e$	K_F	3.15	94.90
		$1/n$	0.52	0.23
		R^2	0.95	0.99
Temkin	$q_e = \beta_1 \ln K_T + \beta_1 \ln C_e$	β_1	32.58	57.57
		K_T (L mg^{-1})	0.036	2.12
		R^2	0.98	0.91

CR onto the c-DAC surface might form a heterogeneous coverage due to the uneven distribution of the cationic sites ($-N^+(CH_3)_3$) on the adsorbent's surface.[56] Furthermore, the favorability of CR adsorption on both DAC and c-DAC could be confirmed by the separation factor value (R_L) of the Langmuir model ($0 < R_L < 1$) and the adsorption intensity value ($1/n$) of the Freundlich model ($0 < 1/n < 1$).[57] In contrast, the relatively low correlation coefficient values using the Temkin isotherm model indicated that the experimental data do not follow this isotherm approach.

In this study, the CR maximum adsorption capacity q_{max} determined by using the Langmuir model was found to be 154.8 and 540.5 mg/g for DAC and c-DAC, respectively, all close to the experimental maximum adsorption values $q_{max,exp}$.

https://doi.org/10.1021/acsomega.2c07839
ACS Omega 2023, 8, 8634−8649

A comparison in terms of the $q_{max,exp}$ values for DAC and c-DAC with those from other cellulose-based adsorbents in recently published studies is shown in Table 5. It was seen that

Table 5. Comparison of the Maximum Adsorption Capacities (q_{max}) of Different Functionalized Cellulose-Based Adsorbents for Congo Red Removal

cellulose-based adsorbents	q_{max} (mg/g)	pH	refs
epichlorohydrin cross-linked dialdehyde cellulose	34.7	7	59
cellulose/chitosan hydrogel beads regenerated from ionic liquid	40	4	60
poly(*N*,*N*-dimethylacrylamide-*co*-acrylamide) grafted cellulose hydrogel	102.4	4.5	61
dialdehyde microfibrillated cellulose/chitosan film	152.5	5.5	45
cellulose/chitosan aerogel	381.7	7	62
positive surfactant (CTAB) modified cellulose nanocrystal	448.4	7.5	63
zwitterion moiety modified cellulose	541.8	6	23
imidazolium ionic liquid modified cellulose	563	7	22
regenerated cellulose-chitosan foam	1170.2	7.4	58
dialdehyde cellulose (DAC)	129.6	7	this study
cationic dialdehyde cellulose modified by Girard's reagent T (c-DAC)	540.3	7	this study

the c-DAC adsorbent exhibited a very high q_{max} value, comparable to the best reported nanostructured cellulose-based materials. Although the q_{max} value of DAC is lower than that of c-DAC in this study, the demonstrated DAC sample is still better than the epichlorohydrin cross-linked dialdehyde cellulose sample which has a similar chemical structure. Perhaps the difference is due to the higher surface area in our DAC sample. The performance of c-DAC is lower than that of some regenerated cellulose materials.[48,58]

Effect of Ionic Strength. In the textile industry, high concentrations of varying inorganic salts (e.g., sodium chloride and sodium sulfate) are often used as dyeing promoters. Therefore, the effect of varying anionic ions (i.e., Cl^-, SO_4^{2-}, and PO_4^{3-}) on the adsorption performance of DAC and c-DAC toward CR was investigated, and the results are shown in Figure 10. It was interesting to find that when the salt concentration increased from 0 to 0.3 M, the q_e value of DAC increased by about 5.9-fold (from 32.2 to 189.5−195.2 mg/g), while that of c-DAC increased by about 1.5-fold (from 134.0 to 190.6−198.7 mg/g). Theoretically, when the electrostatic interaction between the adsorbent surface and adsorbate molecules is repulsive, an increase in the ionic strength can improve adsorption performance. Conversely, if the electrostatic interaction between them is attractive, an increase in ionic strength can decrease the adsorption performance.[64] This can explain the significant increase of the CR adsorption value by negatively charged DAC. However, we note that the electrostatic interaction between c-DAC and CR is attractive, but no decrease in the adsorption performance was found when the ionic strength was increased. According to Alberghina et al.,[65] the inclusion of the positive counterions (gegenions) could decrease the mutual repulsive force between dye molecules and promote dye−dye dimerization. Meanwhile, in more concentrated solutions, the intermolecular forces between the dye molecules (i.e., van der Waals force, ion−dipole, and dipole−dipole interactions) would increase due to the destruction of the hydration shell, thereby increasing the dye aggregation.[65] Tang and Al-Degs have also reported an increase in dye adsorption value with increasing salt concentration in the system.[64,66]

3.2.4. Desorption and Recyclability Study. The recyclability of the c-DAC adsorbent for CR removal was estimated through continuous cycling of the adsorption−desorption process five times, and the results are shown in Figure 11a. As c-DAC exhibited excellent adsorption capability in strong alkalinity, the commonly used sodium hydroxide was not used as a suitable desorption eluent here. Instead, a 1:1 ratio of ethanol and 0.1 M NaOH mixture was used as an effective desorption eluent to remove CR from c-DAC. However, the desorption efficiency of CR was found to decrease from 71.9% to 52.6% after five cycles, indicating some adsorption sites on the c-DAC surface might have reacted with CR and formed irreversible adsorption. Nevertheless, after five adsorption−desorption cycles, the adsorption q_e value of c-DAC was 62.5 mg/g, remaining at 86.9% of the initial adsorption q_e value in cycle 1 (72.0 mg/g). The decrease in the adsorption value may be attributed to the loss of the adsorbent during washing and/or incomplete desorption. Overall, this study indicates that c-DAC can be effectively regenerated and reused for CR removal from an aqueous solution and has considerable potential in wastewater treatment applications.

3.2.5. Column Adsorption Study. In order to explore DAC and c-DAC's usage in a practical wastewater treatment setting, a column adsorption study was carried out via a continuous flow of dye solution through a fixed height column to estimate

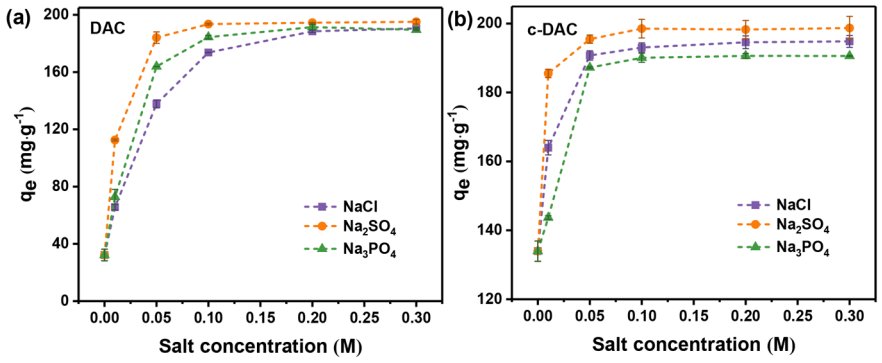

Figure 10. Effect of different salt concentration (NaCl, Na_2SO_4, and Na_3PO_4) on the equilibrium CR adsorption value by (a) DAC and (b) c-DAC (C_0 = 100 mg/L, pH 7).

https://doi.org/10.1021/acsomega.2c07839
ACS Omega 2023, 8, 8634−8649

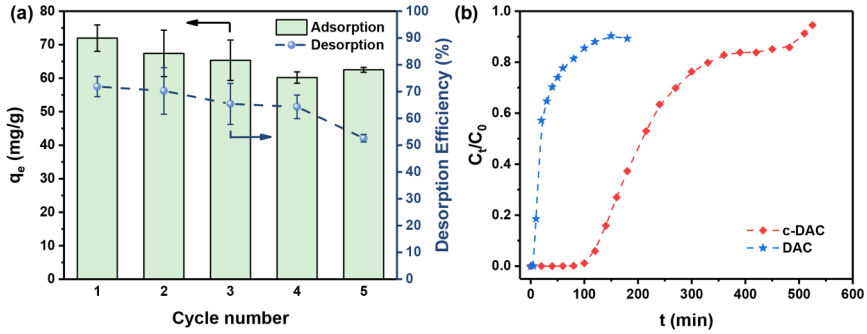

Figure 11. (a) Recyclability of c-DAC for CR adsorption (C_0 = 100 mg/L, pH 7). (b) Breakthrough curves of CR removal by DAC and c-DAC using fixed-bed columns (C_0 = 100 mg/L, pH 7, H = 3 cm, Q = 2 mL/min).

the dynamic adsorption performance of different adsorbents for the CR removal. The breakthrough curves for the CR removal by DAC and c-DAC are plotted in Figure 11b, and the relevant parameters obtained in this study are listed in Table 6.

Table 6. DAC and c-DAC Column Adsorption Data and Relevant Parameters for CR Removal

adsorbent	t_b (min)	t_e (min)	q_{tot} (mg)	q_{eq} (mg/g)	M_{tot}(mg)	R(%)
DAC	10	150	7.3	14.6	30	24.3
c-DAC	140	510	49.7	99.4	102	48.7

In this table, the breakthrough time t_b and the exhaustion time t_e represent the time at which C_t/C_0 = 0.1 and 0.9, respectively. It was seen that exhaustion occurred quickly in the DAC bed (ca. 150 min), while the c-DAC bed possesses much longer t_e (ca. 510 min). The removal efficiency (R) of DAC and c-DAC bed for CR was 24.3% and 48.7%, respectively. It is believed that the column bed removal efficiency could be enhanced by increasing the bed height and/or decreasing the flow rate and the initial dye concentration.[33] A detailed study regarding the effects of column setup conditions on the dynamic dye removal efficiency will be conducted in the future. The preliminary column study confirmed the rapid interaction between CR and c-DAC due to the abundant active sites on the c-DAC surface. The study further indicated that c-DAC can be used as a potential biosorbent for removal of CR and other anionic dyes with the fixed-bed column format in a practical setting.

4. CONCLUSIONS

Anionic and cationic dialdehyde nanostructured cellulose adsorbents (DAC and c-DAC) were successfully prepared and examined for removal or separation of different organic dyes through the adsorption process. The physical and chemical properties of DAC and c-DAC were characterized by FT-IR, ^{13}C NMR, WAXD, BET surface areas, SEM, TEM, CNS elemental analysis, and zeta potential measurements. DAC exhibited superior adsorption capability toward cationic dyes (BBY and BCB), while c-DAC showed superior adsorption capability toward anionic dyes (CR, AG25, ABM, and ARS). Both DAC and c-DAC could be used to separate the high-affinity dyes of opposite charges in binary mixtures. The good adsorption capability toward different dyes can be attributed to two main driving forces between the modified cellulose surface and the dye molecules: (1) the covalent bond formation between the aldehyde groups on cellulose and the amino groups on dyes (through Schiff's base reaction) and (2) electrostatic interaction. The effects of contact time, initial pH, ionic strength, and initial dye concentration on the CR (containing both cationic amino and anionic sulfonate groups) adsorption were investigated systematically. The results showed that both DAC and c-DAC could adsorb CR well even under strong alkalinity or at high salt concentrations, with the maximum adsorption capacity of 129.6 and 540.3 mg/g, respectively, which are comparable to many of the best nanocellulose-based adsorbents in the literature. The adsorption kinetic data from both DAC and c-DAC could be described well by the pseudo-second-order kinetic model, but the equilibrium adsorption results for DAC and c-DAC were found to be fitted best using Langmuir and Freundlich isotherm models, respectively, perhaps due to the difference in functionality distribution on the cellulose surface. Finally, c-DAC exhibited decent recyclability (using five-cycle testing) and showed good performance using the column adsorption test, indicating that members of this family of nanocellulose adsorbents are promising candidates for effective dye removal or separation in treating industrial wastewater.

■ ASSOCIATED CONTENT

Supporting Information

The Supporting Information is available free of charge at https://pubs.acs.org/doi/10.1021/acsomega.2c07839.

Descriptions of the methods used to determine the aldehyde content in DAC/c-DAC samples by titration and the degree of GT substitution on c-DAC; calibration curves of different dyes; nitrogen adsorption−desorption isotherms of the DAC and c-DAC samples; peak deconvolution of the WAXD profiles for pristine_cellulose, DAC, and c-DAC samples (PDF)

■ AUTHOR INFORMATION

Corresponding Author

Benjamin S. Hsiao − *Department of Chemistry, Stony Brook University, Stony Brook, New York 11794, United States;* orcid.org/0000-0002-3180-1826; Phone: +1(631)632-7793; Email: benjamin.hsiao@stonybrook.edu

Authors

Xiangyu Huang − *Department of Chemistry, Stony Brook University, Stony Brook, New York 11794, United States*

Pejman Hadi − *Department of Chemistry, Stony Brook University, Stony Brook, New York 11794, United States*

Ritika Joshi − *Department of Chemistry, Stony Brook University, Stony Brook, New York 11794, United States*

https://doi.org/10.1021/acsomega.2c07839
ACS Omega 2023, 8, 8634−8649

Abdulrahman G. Alhamzani − *Department of Chemistry, Imam Mohammad Ibn Saud Islamic University, Riyadh 11623, Saudi Arabia*

Complete contact information is available at: https://pubs.acs.org/10.1021/acsomega.2c07839

Notes

The authors declare no competing financial interest.

■ ACKNOWLEDGMENTS

This work was supported by the Polymer Program from the Division of Materials Science of National Science Foundation (NSF-DMR- 2216585) and the Center for Clean Water Technology from the New York State Department of Environmental Conservation. The authors also extend their appreciation to the Deanship of Scientific Research at Imam Mohammad Ibn Saud Islamic University for funding through Research Partnership Program (RP-21-09-67). The authors thank Dr. Kai Chi for his experimental assistance. The SEM and TEM experiments were carried out in the Advanced Energy Research and Technology Center (AERTC) and Central Microscopy Imaging Center (CMIC) facilities at Stony Brook University.

■ REFERENCES

(1) Tara, N.; Siddiqui, S. I.; Rathi, G.; Chaudhry, S. A.; Inamuddin; Asiri, A. M. Nano-engineered Adsorbent for the Removal of Dyes from Water: A Review. *Current Analytical Chemistry* **2020**, *16* (1), 14−40.

(2) Abdi, J.; Vossoughi, M.; Mahmoodi, N. M.; Alemzadeh, I. Synthesis of metal-organic framework hybrid nanocomposites based on GO and CNT with high adsorption capacity for dye removal. *Chem. Eng. J.* **2017**, *326*, 1145−1158.

(3) Singh, R. L.; Singh, P. K.; Singh, R. P. Enzymatic decolorization and degradation of azo dyes−A review. *International Biodeterioration & Biodegradation* **2015**, *104*, 21−31.

(4) Chiam, S. L.; Pung, S. Y.; Yeoh, F. Y. Recent developments in MnO2-based photocatalysts for organic dye removal: a review. *Environ. Sci. Pollut Res. Int.* **2020**, *27* (6), 5759−5778.

(5) Hassan, M. M.; Carr, C. M. A critical review on recent advancements of the removal of reactive dyes from dyehouse effluent by ion-exchange adsorbents. *Chemosphere* **2018**, *209*, 201−219.

(6) Chen, B.; Jiang, C.; Yu, D.; Wang, Y.; Xu, T. Design of an alternative approach for synergistic removal of multiple contaminants: Water splitting coagulation. *Chem. Eng. J.* **2020**, *380*, 122531.

(7) Abdel-Karim, A.; El-Naggar, M. E.; Radwan, E.; Mohamed, I. M.; Azaam, M.; Kenawy, E.-R. High-performance mixed-matrix membranes enabled by organically/inorganic modified montmorillonite for the treatment of hazardous textile wastewater. *Chem. Eng. J.* **2021**, *405*, No. 126964.

(8) Ganiyu, S. O.; Brito, L. R. D.; de Araújo Costa, E. C. T.; dos Santos, E. V.; Martínez-Huitle, C. A. Solar photovoltaic-battery system as a green energy for driven electrochemical wastewater treatment technologies: Application to elimination of Brilliant Blue FCF dye solution. *J. Environ. Chem. Eng.* **2019**, *7* (1), 102924.

(9) Katheresan, V.; Kansedo, J.; Lau, S. Y. Efficiency of various recent wastewater dye removal methods: A review. *J. Environ. Chem. Eng.* **2018**, *6* (4), 4676−4697.

(10) Liu, H.; Sun, R.; Feng, S.; Wang, D.; Liu, H. Rapid synthesis of a silsesquioxane-based disulfide-linked polymer for selective removal of cationic dyes from aqueous solutions. *Chem. Eng. J.* **2019**, *359*, 436−445.

(11) El-Naggar, M. E.; Radwan, E. K.; Rashdan, H. R.; El-Wakeel, S. T.; Koryam, A. A.; Sabt, A. Simultaneous removal of Pb 2+ and direct red 31 dye from contaminated water using N-(2-hydroxyethyl)-2-oxo-2 H-chromene-3-carboxamide loaded chitosan nanoparticles. *RSC Adv.* **2022**, *12* (29), 18923−18935.

(12) Li, Y.; Yan, X.; Hu, X.; Feng, R.; Zhou, M. Trace pyrolyzed ZIF-67 loaded activated carbon pellets for enhanced adsorption and catalytic degradation of Rhodamine B in water. *Chem. Eng. J.* **2019**, *375*, 122003.

(13) Ranote, S.; Chauhan, G. S.; Joshi, V. Etherified Moringa oleifera gum as rapid and effective dye adsorbents. *Chem. Eng. J.* **2020**, *387*, 124055.

(14) Fadillah, G.; Saleh, T. A.; Wahyuningsih, S.; Ninda Karlina Putri, E.; Febrianastuti, S. Electrochemical removal of methylene blue using alginate-modified graphene adsorbents. *Chem. Eng. J.* **2019**, *378*, 122140. Robati, D.; Mirza, B.; Rajabi, M.; Moradi, O.; Tyagi, I.; Agarwal, S.; Gupta, V. K. Removal of hazardous dyes-BR 12 and methyl orange using graphene oxide as an adsorbent from aqueous phase. *Chem. Eng. J.* **2016**, *284*, 687−697.

(15) Kyzas, G. Z.; Lazaridis, N. K.; Mitropoulos, A. C. Removal of dyes from aqueous solutions with untreated coffee residues as potential low-cost adsorbents: Equilibrium, reuse and thermodynamic approach. *Chem. Eng. J.* **2012**, *189*−*190*, 148−159.

(16) Li, D.; Tian, X.; Wang, Z.; Guan, Z.; Li, X.; Qiao, H.; Ke, H.; Luo, L.; Wei, Q. Multifunctional adsorbent based on metal-organic framework modified bacterial cellulose/chitosan composite aerogel for high efficient removal of heavy metal ion and organic pollutant. *Chem. Eng. J.* **2020**, *383*, 123127.

(17) Zhang, C.; Li, P.; Huang, W.; Cao, B. Selective adsorption and separation of organic dyes in aqueous solutions by hydrolyzed PIM-1 microfibers. *Chem. Eng. Res. Des.* **2016**, *109*, 76−85.

(18) Ahmadijokani, F.; Mohammadkhani, R.; Ahmadipouya, S.; Shokrgozar, A.; Rezakazemi, M.; Molavi, H.; Aminabhavi, T. M.; Arjmand, M. Superior chemical stability of UiO-66 metal-organic frameworks (MOFs) for selective dye adsorption. *Chem. Eng. J.* **2020**, *399*, 125346. Zhang, J.; Li, F.; Sun, Q. Rapid and selective adsorption of cationic dyes by a unique metal-organic framework with decorated pore surface. *Appl. Surf. Sci.* **2018**, *440*, 1219−1226.

(19) Koryam, A. A.; El-Wakeel, S. T.; Radwan, E. K.; Darwish, E. S.; Abdel Fattah, A. M. One-Step Room-Temperature Synthesis of Bimetallic Nanoscale Zero-Valent FeCo by Hydrazine Reduction: Effect of Metal Salts and Application in Contaminated Water Treatment. *ACS omega* **2022**, *7* (39), 34810−34823.

(20) Sharma, P. R.; Sharma, S. K.; Lindström, T.; Hsiao, B. S. Nanocellulose-Enabled Membranes for Water Purification: Perspectives. *Advanced Sustainable Systems* **2020**, *4* (5), 1900114. Voisin, H.; Bergström, L.; Liu, P.; Mathew, A. P. Nanocellulose-based materials for water purification. *Nanomaterials* **2017**, *7* (3), 57.

(21) Shaheen, T. I.; Radwan, E. K.; El-Wakeel, S. T. Unary and binary adsorption of anionic dye and toxic metal from wastewater using 3-aminopropyltriethoxysilane functionalized porous cellulose acetate microspheres. *Microporous Mesoporous Mater.* **2022**, *338*, 111996.

(22) Zhang, S.-F.; Yang, M.-X.; Qian, L.-W.; Hou, C.; Tang, R.-H.; Yang, J.-F.; Wang, X.-C. Design and preparation of a cellulose-based adsorbent modified by imidazolium ionic liquid functional groups and their studies on anionic dye adsorption. *Cellulose* **2018**, *25* (6), 3557−3569.

(23) Laureano-Anzaldo, C. M.; Haro-Mares, N. B.; Meza-Contreras, J. C.; Robledo-Ortíz, J. R.; Manríquez-González, R. Chemical modification of cellulose with zwitterion moieties used in the uptake of red Congo dye from aqueous media. *Cellulose* **2019**, *26* (17), 9207−9227.

(24) Zhu, W.; Liu, L.; Liao, Q.; Chen, X.; Qian, Z.; Shen, J.; Liang, J.; Yao, J. Functionalization of cellulose with hyperbranched polyethylenimine for selective dye adsorption and separation. *Cellulose* **2016**, *23* (6), 3785−3797.

(25) Mehltretter, C. Some landmarks in the chemical technology of carbohydrate oxidation. *Starch-Stärke* **1963**, *15* (9), 313−319.

(26) Sirviö, J.; Honka, A.; Liimatainen, H.; Niinimäki, J.; Hormi, O. Synthesis of highly cationic water-soluble cellulose derivative and its

potential as novel biopolymeric flocculation agent. *Carbohydr. Polym.* **2011**, *86* (1), 266−270.
(27) Huang, X.; Dognani, G.; Hadi, P.; Yang, M.; Job, A. E.; Hsiao, B. S. Cationic Dialdehyde Nanocellulose from Sugarcane Bagasse for Efficient Chromium(VI) Removal. *ACS Sustainable Chem. Eng.* **2020**, *8* (12), 4734−4744.
(28) Liimatainen, H.; Sirviö, J.; Pajari, H.; Hormi, O.; Niinimäki, J. Regeneration and recycling of aqueous periodate solution in dialdehyde cellulose production. *J. Wood Chem. Technol.* **2013**, *33* (4), 258−266.
(29) Veelaert, S.; De Wit, D.; Gotlieb, K.; Verhé, R. Chemical and physical transitions of periodate oxidized potato starch in water. *Carbohydr. Polym.* **1997**, *33* (2−3), 153−162.
(30) Park, S.; Baker, J. O.; Himmel, M. E.; Parilla, P. A.; Johnson, D. K. Cellulose crystallinity index: measurement techniques and their impact on interpreting cellulase performance. *Biotechnol. Biofuels* **2010**, *3*, 10.
(31) Elazzouzi-Hafraoui, S.; Nishiyama, Y.; Putaux, J. L.; Heux, L.; Dubreuil, F.; Rochas, C. The shape and size distribution of crystalline nanoparticles prepared by acid hydrolysis of native cellulose. *Biomacromolecules* **2008**, *9* (1), 57−65. Chi, K.; Catchmark, J. M. The influences of added polysaccharides on the properties of bacterial crystalline nanocellulose. *Nanoscale* **2017**, *9* (39), 15144−15158.
(32) Luo, X.; Yuan, J.; Liu, Y.; Liu, C.; Zhu, X.; Dai, X.; Ma, Z.; Wang, F. Improved Solid-Phase Synthesis of Phosphorylated Cellulose Microsphere Adsorbents for Highly Effective Pb2+ Removal from Water: Batch and Fixed-Bed Column Performance and Adsorption Mechanism. *ACS Sustainable Chem. Eng.* **2017**, *5* (6), 5108−5117.
(33) Ji, F.; Li, C.; Xu, J.; Liu, P. Dynamic adsorption of Cu(II) from aqueous solution by zeolite/cellulose acetate blend fiber in fixed-bed. *Colloids Surf., A* **2013**, *434*, 88−94.
(34) Xu, G.; Wang, L.; Liu, J.; Wu, J. FTIR and XPS analysis of the changes in bamboo chemical structure decayed by white-rot and brown-rot fungi. *Appl. Surf. Sci.* **2013**, *280*, 799−805. Liu, X.; Wang, L.; Song, X.; Song, H.; Zhao, J. R.; Wang, S. A kinetic model for oxidative degradation of bagasse pulp fiber by sodium periodate. *Carbohydr. Polym.* **2012**, *90* (1), 218−223.
(35) Anjali, T. Modification of carboxymethyl cellulose through oxidation. *Carbohydr. Polym.* **2012**, *87* (1), 457−460.
(36) El-Ayaan, U.; Kenawy, I. M.; El-Reash, Y. G. Synthesis, thermal and spectral. studies of first-row transition metal complexes with Girard-T reagent-based ligand. *J. Mol. Struct.* **2007**, *871* (1−3), 14−23.
(37) Yang, H.; van de Ven, T. G. M. Preparation of hairy cationic nanocrystalline cellulose. *Cellulose* **2016**, *23* (3), 1791−1801.
(38) Sun, Y.; Lin, L.; Deng, H.; Li, J.; He, B.; Sun, R.; Ouyang, P. Structural changes of bamboo cellulose in formic acid. *BioResources* **2008**, *3* (2), 297−315.
(39) Spoljaric, S.; Salminen, A.; Luong, N. D.; Seppälä, J. Ductile nanocellulose-based films with high stretchability and tear resistance. *Eur. Polym. J.* **2015**, *69*, 328−340.
(40) Kim, U.-J.; Kuga, S.; Wada, M.; Okano, T.; Kondo, T. Periodate oxidation of crystalline cellulose. *Biomacromolecules* **2000**, *1* (3), 488−492.
(41) French, A. D. Idealized powder diffraction patterns for cellulose polymorphs. *Cellulose* **2014**, *21* (2), 885−896.
(42) Sun, B.; Hou, Q.; Liu, Z.; Ni, Y. Sodium periodate oxidation of cellulose nanocrystal and its application as a paper wet strength additive. *Cellulose* **2015**, *22* (2), 1135−1146.
(43) Newman, R. H. Carbon-13 NMR evidence for cocrystallization of cellulose as a mechanism for hornification of bleached kraft pulp. *Cellulose* **2004**, *11* (1), 45−52.
(44) Wen, X.; Zheng, Y.; Wu, J.; Wang, L. N.; Yuan, Z.; Peng, J.; Meng, H. Immobilization of collagen peptide on dialdehyde bacterial cellulose nanofibers via covalent bonds for tissue engineering and regeneration. *Int. J. Nanomedicine* **2015**, *10*, 4623−4637.
(45) Zheng, X.; Li, X.; Li, J.; Wang, L.; Jin, W.; Liu, J.; Pei, Y.; Tang, K. Efficient removal of anionic dye (Congo red) by dialdehyde microfibrillated cellulose/chitosan composite film with significantly improved stability in dye solution. *Int. J. Biol. Macromol.* **2018**, *107*, 283−289.
(46) Lei, Z.; Gao, W.; Zeng, J.; Wang, B.; Xu, J. The mechanism of Cu (II) adsorption onto 2,3-dialdehyde nano-fibrillated celluloses. *Carbohydr. Polym.* **2020**, *230*, No. 115631.
(47) Lagergren, S. About the theory of so-called adsorption of soluble substances. *K. Sven. Vetenskapsakad. Handl.* **1898**, *24*, 1−39. Ho, Y. S.; McKay, G. Pseudo-second order model for sorption processes. *Process Biochem.* **1999**, *34* (5), 451−465. Weber, W. J.; Morris, J. C. Kinetics of adsorption on carbon from solution. *J. Sanit. Eng. Div.* **1963**, *89* (2), 31−60.
(48) Kim, U. J.; Kimura, S.; Wada, M. Highly enhanced adsorption of Congo red onto dialdehyde cellulose-crosslinked cellulose-chitosan foam. *Carbohydr. Polym.* **2019**, *214*, 294−302.
(49) Zhou, C.; Wu, Q.; Lei, T.; Negulescu, I. I. Adsorption kinetic and equilibrium studies for methylene blue dye by partially hydrolyzed polyacrylamide/cellulose nanocrystal nanocomposite hydrogels. *Chem. Eng. J.* **2014**, *251*, 17−24.
(50) Tanzifi, M.; Yaraki, M. T.; Kiadehi, A. D.; Hosseini, S. H.; Olazar, M.; Bharti, A. K.; Agarwal, S.; Gupta, V. K.; Kazemi, A. Adsorption of Amido Black 10B from aqueous solution using polyaniline/SiO2 nanocomposite: Experimental investigation and artificial neural network modeling. *J. Colloid Interface Sci.* **2018**, *510*, 246−261.
(51) Tao, J.; Xiong, J.; Jiao, C.; Zhang, D.; Lin, H.; Chen, Y. Hybrid Mesoporous Silica Based on Hyperbranch-Substrate Nanonetwork as Highly Efficient Adsorbent for Water Treatment. *ACS Sustainable Chem. Eng.* **2016**, *4* (1), 60−68. Panczyk, T.; Wolski, P.; Jagusiak, A.; Drach, M. Molecular dynamics study of Congo red interaction with carbon nanotubes. *RSC Adv.* **2014**, *4* (88), 47304−47312.
(52) Hermanson, G. T. *Bioconjugate Techniques*; Academic Press, 2013.
(53) Yuan, B.; Qiu, L. G.; Su, H. Z.; Cao, C. L.; Jiang, J. H. Schiff base - Chitosan grafted L-monoguluronic acid as a novel solid-phase adsorbent for removal of congo red. *Int. J. Biol. Macromol.* **2016**, *82*, 355−360.
(54) Nasuha, N.; Hameed, B. H.; Din, A. T. Rejected tea as a potential low-cost adsorbent for the removal of methylene blue. *J. Hazard. Mater.* **2010**, *175* (1−3), 126−132.
(55) Langmuir, I. The adsorption of gases on plane surfaces of glass, mica and platinum. *Journal of the American Chemical society* **1918**, *40* (9), 1361−1403. Freundlich, H. Über die adsorption in lösungen. *Z. Phys. Chem.* **1907**, *57U* (1), 385−470. Temkin, M. Kinetics of ammonia synthesis on promoted iron catalysts. *Acta physiochim. URSS* **1940**, *12*, 327−356.
(56) Zhong, Q. Q.; Yue, Q. Y.; Li, Q.; Gao, B. Y.; Xu, X. Removal of Cu(II) and Cr(VI) from wastewater by an amphoteric sorbent based on cellulose-rich biomass. *Carbohydr. Polym.* **2014**, *111*, 788−796.
(57) Abouzeid, R. E.; Khiari, R.; El-Wakil, N.; Dufresne, A. Current State and New Trends in the Use of Cellulose Nanomaterials for Wastewater Treatment. *Biomacromolecules* **2019**, *20* (2), 573−597.
(58) Kim, U.-J.; Kim, D.; You, J.; Choi, J. W.; Kimura, S.; Wada, M. Preparation of cellulose-chitosan foams using an aqueous lithium bromide solution and their adsorption ability for Congo red. *Cellulose* **2018**, *25* (4), 2615−2628.
(59) Kumari, S.; Mankotia, D.; Chauhan, G. S. Crosslinked cellulose dialdehyde for Congo red removal from its aqueous solutions. *J. Environ. Chem. Eng.* **2016**, *4* (1), 1126−1136.
(60) Li, M.; Wang, Z.; Li, B. Adsorption behaviour of congo red by cellulose/chitosan hydrogel beads regenerated from ionic liquid. *Desalination and Water Treatment* **2015**, 1−11.
(61) Jana, S.; Pradhan, S. S.; Tripathy, T. Poly(N,N-dimethylacrylamide-co-acrylamide) Grafted Hydroxyethyl Cellulose Hydrogel: A Useful Congo Red Dye Remover. *J. Polym. Environ.* **2018**, *26* (7), 2730−2747.
(62) Wang, Y.; Wang, H.; Peng, H.; Wang, Z.; Wu, J.; Liu, Z. Dye Adsorption from Aqueous Solution by Cellulose/Chitosan Compo-

https://doi.org/10.1021/acsomega.2c07839
ACS Omega 2023, 8, 8634−8649

site: Equilibrium, Kinetics, and Thermodynamics. *Fibers Polym.* **2018**, *19* (2), 340−349.
(63) Ranjbar, D.; Raeiszadeh, M.; Lewis, L.; MacLachlan, M. J.; Hatzikiriakos, S. G. Adsorptive removal of Congo red by surfactant modified cellulose nanocrystals: a kinetic, equilibrium, and mechanistic investigation. *Cellulose* **2020**, *27* (6), 3211−3232.
(64) Aldegs, Y.; Elbarghouthi, M.; Elsheikh, A.; Walker, G. Effect of solution pH, ionic strength, and temperature on adsorption behavior of reactive dyes on activated carbon. *Dyes Pigm.* **2008**, *77* (1), 16−23.
(65) Alberghina, G.; Bianchini, R.; Fichera, M.; Fisichella, S. Dimerization of Cibacron Blue F3GA and other dyes: influence of salts and temperature. *Dyes Pigm.* **2000**, *46* (3), 129−137.
(66) Tang, J.; Zhang, Y.-F.; Liu, Y.; Li, Y.; Hu, H. Efficient ion-enhanced adsorption of congo red on polyacrolein from aqueous solution: Experiments, characterization and mechanism studies. *Sep. Purif. Technol.* **2020**, *252*, 117445.

https://doi.org/10.1021/acsomega.2c07839
ACS Omega 2023, 8, 8634−8649